Sulfatide species with various fatty acid chains in oligodendrocytes at different developmental stages determined by imaging mass spectrometry

Yukie Hirahara[1], Taketoshi Wakabayashi[1], Tetsuji Mori[1, 2], Taro Koike[1], Ikuko Yao[3], Masayuki Tsuda[4], Koichi Honke[5], Hitoshi Gotoh[6], Katsuhiko Ono[6], Hisao Yamada[1]

[1]Department of Anatomy and Cell Science, Kansai Medical University, Osaka, Japan

[2]Faculty of Medicine, Tottori University, Tottori, Japan

[3]Department of Optical Imaging, Institute for Medical Photonics Research, Preeminent Medical Photonics Education & Research Center, Hamamatsu University School of Medicine, Shizuoka, Japan

[4]The Division of Laboratory Animal Science, Science Research Center, [5]Department of Biochemistry, Kochi University Medical School, Kochi, Japan

[6]Department of Biology, Kyoto Prefectural University of Medicine, Kyoto, Japan

Correspondence to: Yukie Hirahara, Department of Anatomy and Cell Science, Kansai Medical University, Shin-machi, Hirakata-City, Osaka, Japan, 573-1010, TEL: 81-72-804-2304 FAX: 81-72-804-2309 E-mail: hirahary@hirakata.kmu.ac.jp

A running title: Sulfatide species in oligodendrocytes

Key words: HSO3-3-galactosylceramide, fatty acid chain, pro-oligodendroblast, myelin, imaging mass spectrometry

Abbreviations: Sulfatide, HSO3-3-galactosylceramide; IMS, imaging mass spectrometry; GalC, galactosylceramide; POA, pro-oligodendroblast antigen; OPCs, Oligodendrocyte progenitor cells; OLs, Oligodendrocytes; MALDI, matrix-assisted laser ionization system; TOF-SIMS, Time-of-Flight Secondary Ion Mass Spectrometry system

Abstract

HSO3-3-galactosylceramide (Sulfatide) species comprise the major glycosphingolipid components of oligodendrocytes and myelin and play functional roles in the regulation of oligodendrocyte maturation and myelin formation. Although various sulfatide species contain different fatty acids, it is unclear how these sulfatide species affect oligodendrogenesis and myelination. The O4 monoclonal antibody reaction with sulfatide has been widely used as a useful marker for oligodendrocytes and myelin. However, sulfatide synthesis during the pro-oligodendroblast stage, where differentiation into the oligodendrocyte lineage has already occurred, has not been examined. Notably, this stage comprises O4-positive cells. In this study, we identified a sulfatide species from the pro-oligodendroblast-to-myelination stage by imaging mass spectrometry (IMS). The results demonstrated that short-chain sulfatides with 16 carbon non-hydroxylated fatty acids (C16) and 18 carbon non-hydroxylated fatty acids (C18) or 18 carbon hydroxylated fatty acids (C18-OH) existed in restricted regions of the early embryonic spinal cord, where pro-oligodendroblasts initially appear, and co-localized with Olig2-positive pro-oligodendroblasts. C18 and C18-OH sulfatides also existed in isolated pro-oligodendroblasts. C22-OH sulfatide became predominant later in oligodendrocyte

development and the longer C24 sulfatide was predominant in the adult brain. Additionally, the presence of each sulfatide species in a different area of the adult brain was demonstrated by IMS at an increased lateral resolution. These findings indicated that O4 recognized sulfatides with short-chain fatty acids in pro-oligodendroblasts. Moreover, the fatty acid chain of the sulfatide became longer as the oligodendrocyte matured. Therefore, individual sulfatide species may have unique roles in oligodendrocyte maturation and myelination.

Introduction

Myelin abundantly consists of two glycosphingolipids—galactosylceramide (GalC) and its sulfated form, sulfatide. GalC makes up 23 wt. % of the total myelin lipid in the central nervous system, while sulfatide makes up 4 wt. % (Norton, 1977). Sommer and Schachner have characterized the oligodendrocyte-reactive monoclonal antibodies (O1 and O4), which were generated by fusing murine myeloma cells with spleen cells that were harvested from mice that had been immunized with bovine corpus callosum (Sommer and Schachner, 1981).

Subsequent studies have demonstrated the antibody reactivities of O1 and O4 with GalC and sulfatide, respectively (Bansal et al., 1989). The $O4^+/O1^-$ stage of the cultured oligodendrocyte precursor has been characterized by its proliferative capacity. However, it enters a state of terminal differentiation with non-migratory characteristics (Gard and Pfeiffer, 1989, 1990). Moreover, the O4-reactive antigen, sulfatide, is undetectable at this stage when $^{35}SO_4$ incorporation is measured in cultured oligodendrocytes or when a TLC analysis is applied (Bansal et al., 1989; Bansal et al., 1992). Therefore, the antigen that reacts with the O4 antibody at the pro-oligodendroblast stage may differ from sulfatide and has been named pro-oligodendroblast antigen (POA) (Bansal et al., 1992).

Oligodendrocyte progenitor cells (OPCs) arise at restricted locations in the ventral ventricular zone during the early embryonic development of the neural tube. They migrate to their final destinations in the brain where they undergo proliferation and subsequently differentiate into myelin-forming cells. These late stage OPCs are also reactive with the O4 antibody (Ono et al., 1995; Miller and Ono, 1998; Ono et al., 2001).

Sulfatide expression is primarily regulated by a synthesizing enzyme, cerebroside sulfotransferase (CST). We have previously generated Cst-null mice that completely lack sulfatide; they exhibit neurological disorders, an abnormal myelin structure and a decrease in axonal ion channel clustering (Honke et al., 2002; Ishibashi et al., 2002). Moreover, the oligodendrocytes of the Cst-null mice exhibit enhanced morphological maturation, and these cells are O4-negative, even at the early stages, which indicates that POA is not synthesized in the absence of this CST enzyme in any brain region. Thus, POA is a sulfated glycolipid that is synthesized by CST and is important for proper oligodendrocyte development (Hirahara et al., 2004). However, its molecular nature remains unclear.

To identify the nature of POA, which starts to express at the critical stage in the oligodendrocyte lineage, it should be important to add a clear description of the specificity of

monoclonal antibody O4. Moreover, the identification of antigen of O4 during all stages of myelination offers the key to an understanding of molecular mechanism at each maturation stage, since O4 has been widely used as a useful marker for oligodendrocyte lineage cells and myelin.

Here, we demonstrate the existence of sulfatide at the pro-oligodendroblast stage. We also show that the sulfatide fatty acid chain length changes during oligodendrocyte development using an imaging mass spectrometry (IMS) technique, which enables the simultaneous visualization of the spatial distribution of numerous biomolecules (Romero-Perez et al., 2014). We initially utilize IMS with a matrix-assisted laser ionization (MALDI) system for a developmental analysis. We subsequently demonstrate the differential spatial distribution of the sulfatide species in the adult brain with a Time-of-Flight Secondary Ion Mass Spectrometry (TOF-SIMS) system. Sulfatide species may have different roles in each oligodendrocyte developmental and myelination stage.

Methods

Reagents and antibodies

Sulfatides and galactocerebrosides from bovine brains, 2,5-Dihydroxybenzoic acid (DHB), the Poly-L-Lysine (PLL) 0.01% solution and 3,3,5-triiodo-L-thyronine (T3) were purchased from Sigma-Aldrich Co. (St. Louis, MO, USA). Carboxymethyl cellulose sodium salt was purchased from WAKO (Osaka, Japan). Mouse monoclonal antibody O4 (clone 81) and anti-myelin basic protein antibody (MAB386) were purchased from Millipore (Temecula, CA, USA). Mouse monoclonal antibody O1 was provided by Dr. K. Ono, Kyoto Prefectural University of Medicine. Mouse monoclonal antibody DI8 (Cheng et al., 2005) and the Cst-null murine brain tissues were provided by Dr. K. Honke, Kochi University Medical School. Anti-Human Olig2 Rabbit IgG was purchased from IBL (Gunma, Japan). Alexa Fluor 488-labeled anti-mouse IgG, Alexa Fluor 488-labeled anti-mouse IgM, Alexa Fluor 633-labeled anti-mouse IgM, Alexa Fluor 488-labeled anti-rabbit IgG and Alexa Fluor 555-labeled anti-mouse IgG were purchased from Thermo Fischer Scientific (Waltham, MA, USA). Cy5-conjugated donkey anti-rabbit IgG was purchased from Jackson ImmunoResearch Laboratories (West Grove, PA). Insulin-Transferrin-Selenium-X and Dulbecco's Modified Eagle's Medium (DMEM) (high glucose) were purchased from Thermo Fischer Scientific (Waltham, MA, USA). HyClone™ Fetal Bovine Serum (FBS) was purchased from GE Healthcare (Logan, Utah, USA).

9-Acridinylamine (9AA) was purchased from Merck KGaA (Darmstadt, Germany). Trifluoroacetic acid (HLC-SOL) was purchased from Kanto Chemical Co., Inc. (Tokyo, Japan). Hoechst 33258 and Dithiothreitol (DTT) were purchased from Nacalai Tesuque (Kyoto, Japan).

Animal care

All animal experiments were conducted in strict accordance with the institutional guidelines of the National Institutes of Health and the Guide for the Care and Use of Laboratory Animals of the National Institutes of Health. Animal care, maintenance, and surgeries were conducted in full compliance with the regulatory standards for the animal research facilities of the Animal Ethics Committee of Kansai Medical University and Kochi University. Adult female Wistar rats and male ICR mice were purchased from Shimizu Laboratory Supplies (Kyoto, Japan) and were housed in plastic cages with standard bedding and continuous access to food and water. The temperature was maintained at 22°C under standard light conditions with a 12-hr light/dark cycle. Fertilized chicken eggs were purchased by Yamagishi (Mie, Japan) and incubated at 38°C. The embryonic stage was determined as described by Hamburger and Hamilton (1951).

Primary cultures of cortical oligodendrocytes

Cerebral hemispheres from E18 rats were mechanically dissociated, plated on 0.01% PLL-coated T75 flasks in DMEM, supplemented with 15% FBS, and cultured. After 15 days, the OPCs were purified from the mixed glial culture by differential shaking. The flasks were shaken at 180 rpm at 37°C for 2 hr to remove non-glial cells; the medium was changed to fresh DMEM supplemented with 10% FBS that had been pre-equilibrated with CO_2, and the flasks were shaken overnight to lift the OPCs from the flasks. The collected cells were seeded onto uncoated culture dishes at 37°C for 2 hr to remove contaminating cells, which had attached to the uncoated plastic dish. The enriched OPCs were collected and seeded onto PLL-coated dishes at 0.5×10^3 cells per 100 mm^2 in MEMα with Insulin-Transferrin-Selenium-X and Glutamax I supplements, 0.4% glucose, 30 ng/ml T3 and 0.5% FBS (differentiation medium).

Fluorescence activated cell sorting

To isolate the pro-oligodendroblasts, FACS was performed using the FACS Aria (BD Biosciences, Franklin Lakes, NJ, USA) with the DI8 antibody, which was originally cloned as a sulfatide-reactive antibody (Cheng *et al*., 2005), and an O1 antibody. As previously described, purified OPCs were re-seeded onto PLL-coated T25 flasks for 1 day with the differentiation medium. The cells were trypsinized for 5-10 min at 37°C. After terminating the reaction using

serum, the cells were collected and labeled with the primary antibodies, (DI8 IgG3 hybridoma supernatant (1:2) and O1 IgM hybridoma supernatant (1:5)) on ice for 15 min. The cells were collected by centrifugation and washed with PBS, followed by co-labeling with the secondary antibodies (Alexa Fluor 488-labeled anti-mouse IgG and Alexa Fluor 633-labeled anti-mouse IgM). The cells were sorted into several populations using the Forward and Side Scatters. The sorting windows for the DI8+/O1+ and DI8+/O1- cell populations were established after the pro-oligodendroblast state of each sorted population was determined by immunostaining with the DI8 and O1 antibodies.

Tissue preparation for IMS

For MALDI-IMS, the dissected non-fixed tissue was mounted in 2% carboxymethyl cellulose, rapidly frozen using powdered dry ice and cut into 10-μm-thick sections using a cryostat (CM3050 S; Leica, Nussloch, Germany) on conductive ITO-coated slides (Bruker Daltonics, MA). The sample was vapor deposited with 9AA as a negative mode matrix under drying and vacuum conditions. The sublimation of 9AA was performed at 220°C for 9 min using the SVC-700TMSG/7PS80 vacuum vapor depositing equipment (Sanyu Electron, Tokyo, Japan).

For TOF-SIMS, the dissected murine brain was rapidly frozen using powdered dry ice and cut into 10-μm-thick sections using a cryostat (CM3050 S; Leica, Nussloch, Germany) on 13-mm square conductive ITO-MAS-coated (20 Ω) slides (MATSUNAMI, Japan). The slides were dried at -80°C with a Freeze dryer FDU-2200 (EYELA, Japan).

IMS analysis with MALDI by iMScope

A MALDI-IMS analysis was performed with a mass microscope (also known as an iMScope-prototype and referred to as "iMScope" in this study) (Shimadzu, Kyoto, Japan). The FACS-purified pro-oligodendroblast suspensions and the sulfatide reference standard (dissolved in methanol) were spotted onto a stainless plate for analysis by iMScope. IMS analysis was performed using Matrix-assisted laser desorption/ionization mass spectrometry in the negative-reflection mode with an accelerating potential of 20 kV on the iMScope. All samples were analyzed in the negative mode (mass range: *m*/*z* 600 to 1000). The data were analyzed using the Imaging MS Solution™ (Shimadzu, Kyoto, Japan) and BioMap software (Novartis, Basel, Switzerland).

IMS analysis with TOF-SIMS

The samples were analyzed by PHI nanoTOF II at ULVAC-PHI, Inc. in Japan. Bismuth (Bi3++) primary ion beams were applied with an ion current of 6.7 nA (high mass resolution mode) or 0.1 nA (high spatial resolution mode). The negative spectra of the sulfatide species were obtained in the high mass resolution mode for spectral acquisition. The imaging data were obtained in the 5 mm x 3 mm to 100 μm x 100 μm range.

Immunofluorescent labeling with OPC and the myelin marker

Serial sections of tissue for IMS were fixed with 4% formaldehyde, washed in 0.1 M PB and immunostained with anti-Olig2 and anti-Myelin Basic Protein (MBP) at 1:200 in PBS with 0.1% Triton X-100 for 24 h at 4°C. The sections were subsequently washed with PBS and incubated with Alexa Fluor 555-labeled anti-rabbit IgG and Alexa Fluor 488-labeled anti-rat IgG (1:1,000). After washing with 0.1 M PB, the sections were mounted with medium that contained 100 mM DTT, 5 μg/ml Hoechst 33258, 50% glycerol, and PBS (pH 7.4), coverslipped and observed with a confocal laser scanning microscope (LSM 510META, Carl Zeiss, Jena, Germany).

Statistical analysis

The average signal intensity of 20 regions (100 μm x100 μm / ROI, 10 ROI for one

slice) in corpus callosum from each animal was analyzed using the imaging MS solution ™ software. The mass value < 0.04 differences to observed *m/z* values as shown in Table were compared. The comparisons of signal intensity from control vs. CST-null was performed by Student's t-test. Values represent mean ± SD of signal intensity from three adult animals per group.

Results

Schematic summary of oligodendrocyte lineage *in vitro*

Specific antibodies that recognize lipid antigens are used to morphologically identify oligodendrocytes at different stages (Fig. 1). The oligodendrocytes are divided into three stages. During stage I, a morphologically bipolar cell becomes a progenitor cell, which is recognized by an A2B5 antibody that is reactive with the c-series gangliosides GT3. During stage II, the cell contains several branches and is referred to as a pro-oligodendroblast; it is recognized by O4, though the O4 antigen at stage II has not been biochemically identified. The stage III cell contains multiple processes and membrane sheets and is referred to as a myelinating oligodendrocyte; it is recognized by O1 and O4, which react with galactocylceramide and

sulfatide, respectively (Bansal et al., 1989, Bansal et al., 1992, Yamada et al., 1996). O4 recognizes cells throughout the oligodendrocyte lineage, including immature pro-oligodendroblasts and mature myelinating oligodendrocytes. To examine the presence of sulfatide in immature pro-oligodendroblasts, we applied MALDI-IMS (iMScope), which is a suitable tool for a high sensitivity and high resolution lipid distribution analysis (Yuki et al., 2011).

Exact mass value of the sulfatide species in the reference standard with iMScope

We designed the conditions to detect the sulfatide species using an iMScope MALDI-IMS instrument in a pilot experiment. We used 9AA as a matrix for the sulfatide analysis with MALDI-MS in a negative ion mode, according to a previous report (Cheng et al., 2010). To confirm the sulfatide composition of the reference standard, we analyzed a mixture of sulfatide species with various fatty acid chains from bovine brains by iMScope (Fig. 2) and compared it to previously measured values by Cheng et al. (2010) and the Human Metabolome Database (http://www.hmdb.ca/). The MALDI-MS spectral analysis of the reference standard acquired by iMScope indicated the numerous sulfatide variant ions that matched the *m/z* values from Cheng et al. (2010). Therefore, the iMScope spectra of the reference standard demonstrated ions that

corresponded to the major sulfatide species as presented in the table below.

The C24 sulfatide is the major species in the adult murine brain, but sulfatide species are absent in the Cst-null murine brain

To confirm whether the sulfatide species spectra that were acquired by iMScope were accurate, we analyzed the sulfatide spectra from the brains of adult CST-null mice; a previous biochemical analysis has shown that these mice do not synthesize sulfatides (Honke et al., 2002). The iMScope spectra of the major sulfatide species in the adult wild type murine brain indicated the presence of ions with *m/z* values of 806.54, 822.51, 862.57, 878.59, 888.62, 890.64, 904.66 and 906.66, which was in agreement with the major species observed in the bovine brain. The major sulfatide ions occurred at *m/z* 888.62 and *m/z* 890.64, which corresponded to C24:1 and C24 sulfatide, respectively (Fig. 3A). The mass imaging of the sulfatide species in the wild type murine brain demonstrated that the major sulfatide species existed in the striatum and corpus callosum, which contained the most abundant myelinated axon bundles (Fig. 3B). Furthermore, the C24 sulfatide imaging signal predominated. Moreover, mass imaging indicated that phosphatidylserine (PS) (*m/z* 834.52) and Phosphatidylinositol (PI) (*m/z* 885.52) (Fig. 3A) were broadly distributed in the brains of both the wild type and Cst-null mice (Fig. 3B). However, the

major sulfatide spectra and the mass imaging signal from the adult Cst-null murine brain completely disappeared, whereas the signaling intensity of PS and PI from the Cst-null murine brain was identical to that of the wild type brain (Fig. 3A, B). Quantities of mass value for sulfatide signal intensity in corpus callosum of the CST-null mouse was also much less compared with the wild type, which is statistically significant (Fig. 3C). Although small amounts of sulfated glyceroglycolipid and d18:1 sphingosine base sulfatide species also existed in the brain (Ishizuka et al., 1978, Cheng et al., 2010), we focused our study on the major sulfatide variant. These findings suggest that the sulfatide species spectra that were acquired by iMScope are accurate. Moreover, the detection methods for sulfatide using iMScope can be used to identify sulfatide in cells at the pro-oligodendroblast stage.

The ion at *m/z* 806.5 is the most abundant species at the pro-oligodendroblast stage

To investigate the existence of sulfatide in pro-oligodendroblast cells, the FACS-sorted pro-oligodendroblasts were analyzed by iMScope. First, we collected pure pro-oligodendroblasts by culturing the OPCs under differentiation conditions and immunostaining them with O4, O1 and DI8; the pro-oligodendroblast stage was identified as O4-positive and O1-negative cells. Because the O1 and O4 antibodies were monoclonal mouse

IgM antibodies, they could not be used for double labeling for isolation via FACS. Therefore, we tested whether the DI8 mouse monoclonal IgG, which was cloned as a sulfatide-reactive antibody (Cheng et al., 2005), could substitute for the O4 mouse monoclonal IgM. DI8-positive cells typically exist in restricted regions of the ventricular zone of the spinal cord in the stage 32 chick embryo, and the ventricular zone has been recognized as the pro-oligodendroblast production area (Fig. 4A, a, b). In culture, the images of the pro-oligodendroblast-stage cells completely overlapped when the cells were stained with DI8 and O4 (Fig. 4B, a-c), in contrast to the O1 and DI8 images (Fig. 4B, d-f). Therefore, DI8 was used for the FACS analysis instead of O4. Furthermore, the pro-oligodendroblast-stage cells were treated with methanol for 30 min at –20°C to characterize the O4/DI8 antigen. The DI8 antigen disappeared from the treated pro-oligodendroblasts, but the GST-π protein, an oligodendrocyte marker, remained unchanged. This indicates that the O4/DI8 antigen may have a lipid component (Fig. 4B, g-i). Finally, the OPCs that were cultured under differentiation conditions were analyzed using the FACS Aria flow cytometer, where they were separated into three fractions based on two parameters—Side Scatter (SSC-A) and Forward Scatter (FSC-A). The separated populations (P1, P2, and P3) were cultured for 1 day and identified by immunostaining and morphological

analysis. P1 comprised noncomplex, medium-sized cells with morphologically immature DI8-positive and O1-negative oligodendrocytes (Fig. 4C, a, b). The morphology of the P2 population, which comprised high-complexity and medium-sized cells, was apparent by phase contrast; the cells exhibited no reactivities with DI8 and O1 (Fig. 4C, a, b). P3 contained high-complexity, large-sized cells and was morphologically represented by mature oligodendrocytes with numerous branches; they were DI8-positive and O1-positive (Fig. 4C, a, b). Double labeling of population P1 with Cy5-conjugated goat anti-mouse IgM for the O1 monoclonal antibody and Alexa 488-conjugated goat anti-mouse IgG for the DI8 monoclonal antibody indicated the following sub-populations: DI8 ^{low} O1^{low} (P4), DI8 ^{high} O1^{low} (P5), and DI8 ^{high} O1^{high} (P6) (Fig. 4C, c). The methanol extract of the sorted P5 population was analyzed for the sulfatide species by iMScope. The spectra from the P5 population indicated ions at *m/z* 806.54 and *m/z* 822.51, which were predicted to be the C18 and C18-OH sulfatides, respectively; PI (*m/z* 885.53) was also present (Fig. 4C, d). These findings suggested that the cultured cells at the pro-oligodendroblast stage contained sulfatides that predominately exhibited C18 chain lengths.

The C16 and C18 sulfatides are located in a defined area of OPC production in the chick

embryonic nervous system

The early development of the oligodendrocyte is well characterized in the embryonic chick brain and spinal cord (Ono et al. 1995, Ono et al. 1997), and O4-positive pro-oligodendroblasts have been identified in a specific region of the ventral zone in the stage 29 embryonic spinal cord. The cells remain there until stage 35, after which they migrate into the dorsal region (Ono et al. 1995).

Using imaging mass spectrometry, we demonstrated that sulfatides existed in specific regions of the stage 32 chick embryonic spinal cord, where pro-oligodendroblasts appeared. The sulfatide species spectra of the section at this stage indicated *m/z* 778.53 as the C16 sulfatide, *m/z* 806.54 as the C18 sulfatide and *m/z* 822.51 as the C18-OH sulfatide (Fig. 5A). O4-positive cells were identified in specific regions of the ventral and lateral parts of the stage 32 spinal cord (Fig. 5B, a, b). Figure 5B, c-h shows the iMScope mass images that were obtained from one slice. The signals from each image at *m/z* 778.5, *m/z* 806.5 and *m/z* 822.5 were clearly present in defined areas of the ventral zone (Fig. 5B, e-g). However, the signal at *m/z* 888.6, the major C24:1 sulfatide of the adult brain (Fig. 3B), was faint (Fig. 5B, h), but the PI signal at *m/z* 885.5 was uniformly distributed (Fig. 5B, d). Moreover, the imaging signal from another section of the

stage 32 spinal cord indicated that the sulfatide species were significantly restricted to a specific area in the ventral zone around the floor plate (Fig. 5B, i), but the PS signal at *m/z* 834.52 had previously spread throughout the whole spinal cord section (Fig. 5B, j).

To confirm whether the restricted area analyzed by iMScope was an OPC production area, serial sections of the stage 38 embryonic spinal cord were analyzed by immunohistochemistry and iMScope. The Olig2 (OPC marker)-positive cell localization pattern was completely matched with the iMScope imaging of the major sulfatide variant, *m/z* 806.5, at the dorsal and ventral regions (Fig. 5C, a, b, d). Sulfatide species at *m/z* 778.5, *m/z* 822.5 and *m/z* 888.6 also co-localized with Olig2 in the ventral region (Fig. 5C, c, e, f). These findings suggested that sulfatide species were synthesized in the area of the first pro-oligodendroblast appearance. At this stage, short-chain sulfatides with 16 and 18 carbon fatty acids were predominant.

Moreover, to further confirm that the *m/z* 806.5 ion that was detected in the embryonic chick spinal cord was a sulfatide variant, a tandem MS analysis of *m/z* 806.5 was performed by iMScope. The tandem MS of the *m/z* 806.5 ion from the embryonic chick spinal cord was compared with that of the adult murine brain (Fig. 6A, a, b). Several fragments of the *m/z* 806.5

ion from the embryonic chick spinal cord, including *m/z* 391.2, *m/z* 409.2, *m/z* 437.2, *m/z* 522.2, *m/z* 551.2 and *m/z* 720.5 (Fig. 6B, b), matched the fragments from the adult murine brain (red arrows in Fig. 6B, b). Fragments *m/z* 522.2 and *m/z* 551.2 were also detected from *m/z* 806.5 in a reference standard of the sulfatide species (data not shown). The coincidence of the fragments suggested that the *m/z* 806.5 ion from the embryonic spinal cord at the pro-oligodendroblast stage was a C18 sulfatide.

The C18-OH sulfatide is predominant during the murine oligodendrocyte developmental stages

Oligodendrocyte precursors appear on the ventral portion of the E14 rat spinal cord and expand to the lateral portion of the midbrain. (Pringle and Richardson, 1993). O4-positive cells are detected in the ventricular surface along the central midline of the cervical spinal cord in whole mount tissue that is derived on E12 and cultured for one day (Wada et al., 2000). To further understand the appearance of the sulfatide species during oligodendrocyte development, we examined embryonic murine brains and spinal cords at different stages. Ions at *m/z* 778.50, *m/z* 806.50, *m/z* 822.53 and *m/z* 878.59 were identified (Fig. 7A, a, b, c, d, e) in the cervical region of the E15.5 spinal cord, whereas *m/z* 888.6, the major sulfatide species in the adult murine

brain (Fig. 3B), was not identified (Fig. 7A, f). The ion at *m/z* 822.53 from the C18-OH sulfatide predominated (Fig. 7A, d), but the C18 sulfatide (*m/z* 806.50) was the main sulfatide in the OPC-producing area of the embryonic chick spinal cord (Fig. 5B, f and 5C, d). The C18-OH sulfatide was also identified along the midline and ventral zone in the caudal region of the E15.5 medulla (Fig. 7A, g, h) and pons (Fig. 7A, i, j). By E18.5, the imaging of *m/z* 806.53 (the C18 sulfatide) and *m/z* 822.50 (the C18-OH sulfatide) revealed that these species had laterally expanded from the midline at the middle region of the medulla (Fig. 7B, a-c) and the caudal region of the pons (Fig. 7B, e-g), in contrast to *m/z* 888.66 (the C24:1 sulfatide) (Fig. 7B, d, h). None of these sulfatides, including the C18, C18-OH or C24:1 sulfatides, were identified in the rostral region of the E18.5 midbrain (Fig. 7B, i-l). In the cervical region of the E19.5 spinal cord, the C18-OH and C22-OH sulfatides appeared at the ventral zone, but the C24:1 sulfatide did not. The stage 37 chick embryo demonstrated that the C18-OH sulfatide distribution expanded toward the dorsal area (Fig. 5C, d). None of the stages and areas had C24 sulfatide species with nonhydroxy and hydroxyl fatty acids or with chain saturated and monounsaturated fatty acids (A,f, B,d,h,l, C,d, for the C24:1 sulfatide; data are not shown for the C24, C24-OH, and C24:1-OH sulfatides). These findings indicate that C18-OH is the major sulfatide during murine

embryogenesis. Moreover, the sulfatide appearance pattern follows the OPC migration pattern that has been previously reported by multiple groups, in which the OPCs that arise from the ventricular foci radially migrate toward the future white matter area (Spassky et al., 1998, Olivier et al., 2001 and Ono et al., 2001). Thus, pro-oligodendroblasts, which have the potential to proliferate and migrate, have short-chain fatty acid sulfatides.

The C18 and C24 sulfatides exhibit patchy distributions in white matter tracts but do not overlap.

To characterize the spatial distributions of the sulfatide species in the adult brain, we monitored the tissue surface distributions of the sulfatide species by TOF-SIMS, which enabled the identification of ion signals at a higher lateral resolution of 100 nm. Previous studies have demonstrated that cholesterol exists in cerebellar white matter, and sulfatide species are uniformly distributed in the white and gray matter of the adult cerebellum (Pernber et al., 2007). However, the presence of each sulfatide species in each oligodendrocyte stage has not been determined. As shown in Figure 7, the sulfatide species in the oligodendrocytes changed during oligodendrocyte development. Thus, we hypothesized that immature oligodendrocytes contained sulfatides with short-chain fatty acids (i.e., C18-sulfatide) and that myelinating

oligodendrocytes had sulfatides with long-chain fatty acids (i.e., C24-sulfatide). Freeze-dried samples of adult murine brains were directly analyzed in a negative mode by PHI nano TOF II. To further dissect the distribution of each sulfatide species, we targeted the isotope variants of the *m/z* 806.5, *m/z* 822.5, *m/z* 862.6 and *m/z* 888.6 ions that were identified by MALDI because detection of natural isotopic molecules would provide stronger intensity signals and facilitate higher resolutions. The area of the corpus callosum that was analyzed is shown (Fig. 8, A, a, b). The serial section was stained with MBP and Olig2 (Fig. 8, A, c. d). The peaks of each variant, which included the natural isotope, were analyzed by TOF-SIMS (Fig. 8, A, e, f). The natural abundance isotopes for the *m/z* 807 ion were demonstrated in the mass spectrum as three isotope peaks (*m/z* 806.55, *m/z* 807.62 and *m/z* 808.55). The *m/z* 823 isotope peaks occurred at *m/z* 822.56, *m/z* 823.65 and *m/z* 824.54. The *m/z* 863 and *m/z* 889 ions were each identified as two isotope ion peaks at *m/z* 862.63, *m/z* 863.63 and *m/z* 888.66, *m/z* 889.64, respectively (Fig. 8, A, e, f). The imaging analysis of the CNO ions, which were expected products of the polypeptide cleavages (Sosnik et al., 2006), exhibited a cell body-like morphology of < 20 μm (Fig. 8, B, a); cholesterol (*m/z* 385; Fig. 8, B, b) was detected in the myelin band (red in Fig. 8, B, d) as previously reported by Pernber et al. 2006. Imaging of the signals from the four sulfatide

species at *m/z* 807, *m/z* 823, *m/z* 863 and *m/z* 889, including each isotope variant, demonstrated a patchy distribution that ran along the axons with a high intensity on the cingulum of the dorsal side of the corpus callosum (Fig. 8, B, c), which correlated with the MBP immunostaining in the same area (Fig. 8, A, c, d). Most sulfatide signals did not overlap with CNO and cholesterol (Fig. 8, B, d). The patchy distributions of < 20 μm per patch for each sulfatide species (Fig. 8, B, e-h) did not merge with one another (Fig. 8, B, i, j). To assess the sulfatide distribution using a higher spatial resolution, the cingulate bundle near the corpus callosum was analyzed (Fig. 8, C, a, b). The cholesterol signals indicated an internode-like morphology (Fig. 8, C, c, d), whereas the sulfatide signals exhibited patchy distributions of < 1 μm through few co-localizations with the cholesterol signals (Fig. 8, C, a-e). This suggested that each sulfatide variant was clustered in a different region of the white matter in the adult brain. The morphological imaging of each sulfatide species in the oligodendrocytes remained unclear, but the patch-like distribution indicated that each sulfatide species spatially dominated a different region.

Discussion

This study is the first to biochemically demonstrate that short-chain fatty acid sulfatides exist

in pro-oligodendroblasts during early embryonic oligodendrogenesis. This finding provides a clear answer regarding the identity of the pro-oligodendroblast O4 antigen, whose biochemical nature had previously been unclear. Sulfatides with short-chain fatty acids participate in the pro-oligodendroblast stage, which is the critical point at which differentiation into an oligodendrocyte lineage cell has occurred.

Oligodendrocyte development progresses through structurally and physiologically distinct stages that are identifiable through the expression of stage-specific antigen, including sphingolipids (Miller et al., 2002). OPCs, which are identified by PDGFR α and Olig2 expression, are induced to proliferate and differentiate into pro-oligodendroblasts, which are immature oligodendrocytes that are recognizable with the O4 antibody. They subsequently develop into mature oligodendrocytes, which are recognizable with O1, and begin to prepare the elongating processes along the axons that form the membrane sheath while undergoing cytoskeletal changes during myelination. We further demonstrate that different sulfatide species occur at different maturation stages and different locations. The sulfatide species at each maturation stage may have different functions with individual roles in the spatial and developmental stages.

The sulfatide composition of the brain has been analyzed using various approaches over multiple decades. In 1964, O'Brien and Rouser (1964) used gas liquid chromatography (GLC) to show that brain tissue had various sulfatide fatty acid species with nonhydroxy and hydroxyl fatty acids, along with odd- and even-chain saturated and monounsaturated fatty acids that contained 14 to 29 carbons. Furthermore, it became clear that the sulfatide fatty acid composition changed with age in the tissue of the human nervous system. The C16 and C18 sulfatides predominated in the newborn brain and gradually decreased with age. The initiation of myelination was followed by a rapid increase in the amount of the long-chain C24 sulfatide and monoenes and a change in the ratio of hydroxy fatty acid to non-hydroxy fatty acid by GLC (Svennerholm and Ställberg-Stenhagen et al., 1968). Various sulfatide species have been analyzed in the rat cerebellum and in multiple sclerosis white matter by negative ion electrospray mass spectrometry; these analyses demonstrated a significant increase in the percentage of hydroxylated C24 sulfatides in multiple sclerosis tissue samples (Marbois et al., 2000). Moreover, C18 sulfatide accumulation in the neurons and astrocytes of arylsulfatase A (ASA)-deficient mice has been demonstrated by quadrupole-time-of-flight mass spectrometry (Isaac et al., 2006) and Matrix-assisted laser desorption/ionization time-of-flight mass

spectrometry (Eckhardt et al., 2007). A powerful high throughput method has recently been reported that describes the direct measurement of sulfatides from tissue extracts by MALDI-MS using 9AA as the matrix; this included the sulfatides identified in the murine brain (Cheng et al., 2010). Moreover, the endogenous sulfatide molecules in the adult brain tissue have been visualized using various methods as follows: the C24 and C18 sulfatide distributions in chemically treated murine brains were determined by TOF-SIMS imaging (Sjövall, et al., 2004); sulfatide variant distributions in the rat cerebellum were assessed by TOF-SIMS imaging (Pernber et al., 2007); C24 sulfatides were detected in rat brain sections via MALDI-IMS imaging (Wang et al., 2008); C24 sulfatides were detected in the middle molecular layer of the rat hippocampus by nanoparticle-assisted laser desorption/ionization-based imaging mass spectrometry (Ageta et al., 2009); sulfatide species detection in the human cerebral cortex was performed by MALDI-IMS (Yuki et al., 2011).

In this study, we used MALDI-IMS to demonstrate that C18 sulfatide existed in immature oligodendrocytes in vivo and at the embryonic stages, whereas C24 sulfatide predominated in the adult brain. We hypothesized that sulfatides with short-chain fatty acids existed in immature oligodendrocytes, and sulfatides with long-chain fatty acid occurred in myelin. Thus, the

specific distribution of each sulfatide variant in the adult brain was examined by TOF-SIMS. Myelin exhibited a strong cholesterol signal in the corpus callosum (Fig. 8) and in the white matter of the cerebellum (Pernber et al., 2007). However, sulfatide signals in the corpus callosum were lower than the cholesterol signal in the corpus callosum (Fig. 8) and in the white matter of the cerebellum (Pernber et al., 2007). Our MALDI imaging demonstrated high C24 sulfatide signals in myelinated areas in the adult brain, including the corpus callosum and internal capsule (Fig. 3). However, the location of the C24 sulfatide signal by TOF-SIMS did not overlap with the high cholesterol signal, which appeared as a specific image of myelinated areas in the corpus callosum (Fig. 8). Difficulties in detecting the ionization of large molecules, such as sulfatides, in the compact myelin lamellae by TOF-SIMS may explain this lack of correlation with cholesterol. The origin of the patchy images that contain each sulfatide remains unclear. However, the result in Figure 8 indicated that each sulfatide species in the corpus callosum of the adult brain localized to a completely different patch, even with small beam size profiling. To demonstrate this localization on the cellular level, further investigations of appropriate ionization conditions for target molecules and high resolution imaging by mass spectrometry will be required to analyze the area dominated by each sulfatide species.

Multiple studies have demonstrated the physiological and pathological functions of different sulfatide species in tissues. An increase in C18 sulfatide levels occurred in neurons following the induction of lethal audiogenic seizures (van Zyl, et al., 2010). Increases in C18 and C18-OH sulfatide levels were observed in the white matter of neonatal rat brains following nitric oxide inhalation, which is a preclinical therapy for brain damage (Olivier, et al., 2010, Kadar, et al., 2014). Ablation of ceramide synthase 1, which catalyzes C18 ceramide synthesis, caused a reduction in myelin-associated glycoprotein levels (Ginkel et al., 2012). In non-nervous system tissues, C16 sulfatide, but not C24 sulfatide, played a role in the inhibition of insulin secretion in beta-cells (Buschard et al., 2006) and was involved in insulin trafficking (Fredman et al., 2000). Moreover, the fatty acid chain lengths of glycosphingolipids, including galactosylceramide, affected fluid cell membranes (Lu et al., 1993). The glycosphingolipid antibody exhibited a higher binding affinity to cells that contained long-chain fatty acid glycosphingolipids over cells that contained shorter fatty acid chain lengths (Kannagi et al., 1982). The increased recognition of the glycosphingolipid's longer acyl chain by the antibody may be due to the increased exposure of the lipid sugar head group on the bilayer surface (Boggs et al., 2004). An aggregation that is based on carbohydrate-carbohydrate interactions

between galactosylceramide-containing liposomes and cerebroside sulfate-containing liposomes depends on the sulfatide fatty acid composition, which is determined by hydroxylation and length (Boggs et al., 2004, Stewart et al., 1993). Here, we demonstrated that the short-chain fatty acid sulfatide species appeared in a defined area of OPC production while the long-chain fatty acid sulfatide species appeared during OL development. Moreover, various sulfatide species were used in the adult mouse. As previously shown, the fatty acid length was closely related to the cell membrane fluid. Therefore, each sulfatide species in the multi-layered compact myelin and in each oligodendrocyte developmental stage might have different functions that should be investigated further.

The sphingoid bases of the galactocylceramide and sulfatide species are primarily d18:1 sphingosine ((2S,3R,4E)-2-amino-4-octadecene-1,3-diol) in the developing rat and human brain (Rosenberg and Stern, 1966, Marbois et al., 2000, Cheng et al., 2010); they include a few d18:0 sphinganine ((2S,3R)-2-aminooctadecane-1,3-diol) forms in the rat brain (Cheng et al., 2010). It has also been reported that 10% of the total sphingoid base content in the murine brain comprises d18:2 sphingadienine ((2S,3R,4E,8E)-2-amino-4,8-octadecadiene-1,3-diol) (Colsch et al., 2004). Sulfatide with a sphingadienine base at m/z 806 has not been reported in the murine brain or in other species (Colsch et al., 2004). Based on previously reported information (Fig. 6), we assume that the m/z 806 ion in the pro-oligodendroblast may be a sulfatide with

N-stearoylsphingosine. Future studies should pursue its actual structure by tandem mass spectrometry.

During myelin formation, sulfatide is required for normal paranodal Axo-Glial Junction formation in the brain (Honke et al., 2002), normal conduction velocity in the sciatic nerve (Hayashi et al., 2013), and normal ion channel clustering on axons (Ishibashi et al., 2002). Moreover, sulfatide is required for proteolipid protein transportation to the myelin membrane in multilayered compact myelin (Baron et al., 2015, Ozgen et al., 2014). Sulfatide participates in carbohydrate–carbohydrate interactions with galactosylceramide between apposed myelin membranes (Boggs, 2014, Boggs et al., 2010, Boggs et al., 2008a) and mediates signal transduction across the membrane to regulate myelin formation and function (Boggs et al., 2008b). In oligodendrocytes, sulfatide serves as a receptor for laminin-2 and mediates oligodendrocyte maturation (Baron et al., 2014). It regulates the number of mature oligodendrocytes at the postnatal stage (Hirahara et al., 2004) and in the adult (Shroff et al., 2009). Therefore, each sulfatide variant may be involved in the spatiotemporal regulation of oligodendrocyte maturation, myelin formation and function, and myelin maintenance.

Acknowledgments

We thank Dr. Joan M. Boggs (Toronto University) for helpful advice, Dr. Itsuko Ishizaki (ULVAC-PHI, Inc.) for assistance with PHI nano TOF II and the analysis, Ms. Yoko Shimotsuma and Mr. Akira Saitou for assistance with MALDI-IMS, Dr. Hideaki Kuge (Kochi

University Medical School) for advice regarding the mass spectrometry of lipids and Dr. Hiroyuki Gonda (Kansai medical university) for assistance with the FACS Aria. This work was supported by Grants-in-Aid for Scientific Research (C), number 26430077 (Y.H.) and number 16K08480 (H.Y) from the Japan Society for the Promotion of Science. The authors have no conflicts of interest to declare.

References

Ageta, H., Asai, S., Sugiura, Y., Goto-Inoue, N., Zaima, N. and Setou, M. (2009) Layer-specific sulfatide localization in rat hippocampus middle molecular layer is revealed by nanoparticle-assisted laser desorption/ionization imaging mass spectrometry. *Med Mol Morphol,* **42,** 16-23.

Bansal, R. and Pfeiffer, S. E. (1992) Novel stage in the oligodendrocyte lineage defined by reactivity of progenitors with R-mAb prior to O1 anti-galactocerebroside. *J Neurosci Res,* **32,** 309-316.

Bansal, R., Stefansson, K. and Pfeiffer, S. E. (1992) Proligodendroblast antigen (POA), a developmental antigen expressed by A007/O4-positive oligodendrocyte progenitors prior to the appearance of sulfatide and galactocerebroside. *J Neurochem,* **58,** 2221-2229.

Bansal, R., Warrington, A. E., Gard, A. L., Ranscht, B. and Pfeiffer, S. E. (1989) Multiple and novel specificities of monoclonal antibodies O1, O4, and R-mAb used in the analysis of oligodendrocyte development. *J Neurosci Res,* **24,** 548-557.

Baron, W., Bijlard, M., Nomden, A., de Jonge, J. C., Teunissen, C. E. and Hoekstra, D. (2014) Sulfatide-mediated control of extracellular matrix-dependent oligodendrocyte maturation. *Glia,* **62,** 927-942.

Baron, W., Ozgen, H., Klunder, B., de Jonge, J. C., Nomden, A., Plat, A., Trifilieff, E., de Vries, H. and Hoekstra, D. (2015) The major myelin-resident protein PLP is transported to

myelin membranes via a transcytotic mechanism: involvement of sulfatide. *Mol Cell Biol,* **35,** 288-302.

Boggs, J. M. (2014) Role of galactosylceramide and sulfatide in oligodendrocytes and CNS myelin: formation of a glycosynapse. *Adv Neurobiol,* **9,** 263-291.

Boggs, J. M., Gao, W. and Hirahara, Y. (2008a) Myelin glycosphingolipids, galactosylceramide and sulfatide, participate in carbohydrate-carbohydrate interactions between apposed membranes and may form glycosynapses between oligodendrocyte and/or myelin membranes. *Biochim Biophys Acta,* **1780,** 445-455.

Boggs, J. M., Gao, W. and Hirahara, Y. (2008b) Signal transduction pathways involved in interaction of galactosylceramide/sulfatide-containing liposomes with cultured oligodendrocytes and requirement for myelin basic protein and glycosphingolipids. *J Neurosci Res,* **86,** 1448-1458.

Boggs, J. M., Gao, W., Zhao, J., Park, H. J., Liu, Y. and Basu, A. (2010) Participation of galactosylceramide and sulfatide in glycosynapses between oligodendrocyte or myelin membranes. *FEBS Lett,* **584,** 1771-1778.

Boggs, J. M., Wang, H., Gao, W., Arvanitis, D. N., Gong, Y. and Min, W. (2004) A glycosynapse in myelin? *Glycoconj J,* **21,** 97-110.

Buschard, K., Blomqvist, M., Månsson, J. E., Fredman, P., Juhl, K. and Gromada, J. (2006) C16:0 sulfatide inhibits insulin secretion in rat beta-cells by reducing the sensitivity of KATP channels to ATP inhibition. *Diabetes,* **55,** 2826-2834.

Cheng, H., Sun, G., Yang, K., Gross, R. W. and Han, X. (2010) Selective desorption/ionization of sulfatides by MALDI-MS facilitated using 9-aminoacridine as matrix. *J Lipid Res,* **51,** 1599-1609.

Cheng, X., Zhang, Y., Kotani, N. et al. (2005) Production of a recombinant single-chain variable-fragment (scFv) antibody against sulfoglycolipid. *J Biochem,* **137,** 415-421.

Colsch, B., Afonso, C., Popa, I., Portoukalian, J., Fournier, F., Tabet, J. C. and Baumann, N. (2004) Characterization of the ceramide moieties of sphingoglycolipids from mouse brain by ESI-MS/MS: identification of ceramides containing sphingadienine. *J Lipid Res,* **45,** 281-286.

Eckhardt, M., Hedayati, K. K., Pitsch, J., Lüllmann-Rauch, R., Beck, H., Fewou, S. N. and Gieselmann, V. (2007) Sulfatide storage in neurons causes hyperexcitability and axonal degeneration in a mouse model of metachromatic leukodystrophy. *J Neurosci,* **27,** 9009-9021.

Fredman, P., Mânsson, J. E., Rynmark, B. M., Josefsen, K., Ekblond, A., Halldner, L., Osterbye, T., Horn, T. and Buschard, K. (2000) The glycosphingolipid sulfatide in the islets of Langerhans in rat pancreas is processed through recycling: possible involvement in insulin trafficking. *Glycobiology,* **10,** 39-50.

Gard, A. L. and Pfeiffer, S. E. (1989) Oligodendrocyte progenitors isolated directly from developing telencephalon at a specific phenotypic stage: myelinogenic potential in a defined environment. *Development,* **106,** 119-132.

Gard, A. L. and Pfeiffer, S. E. (1990) Two proliferative stages of the oligodendrocyte lineage (A2B5+O4- and O4+GalC-) under different mitogenic control. *Neuron,* **5,** 615-625.

Ginkel, C., Hartmann, D., vom Dorp, K. et al. (2012) Ablation of neuronal ceramide synthase 1 in mice decreases ganglioside levels and expression of myelin-associated glycoprotein in oligodendrocytes. *J Biol Chem,* **287,** 41888-41902.

HAMBURGER, V. and HAMILTON, H. L. (1951) A series of normal stages in the development of the chick embryo. *J Morphol,* **88,** 49-92.

Hayashi, A., Kaneko, N., Tomihira, C. and Baba, H. (2013) Sulfatide decrease in myelin influences formation of the paranodal axo-glial junction and conduction velocity in the sciatic nerve. *Glia,* **61,** 466-474.

Hirahara, Y., Bansal, R., Honke, K., Ikenaka, K. and Wada, Y. (2004) Sulfatide is a negative regulator of oligodendrocyte differentiation: development in sulfatide-null mice. *Glia,* **45,** 269-277.

Honke, K., Hirahara, Y., Dupree, J. et al. (2002) Paranodal junction formation and spermatogenesis require sulfoglycolipids. *Proc Natl Acad Sci U S A,* **99,** 4227-4232.

Isaac, G., Pernber, Z., Gieselmann, V., Hansson, E., Bergquist, J. and Månsson, J. E. (2006) Sulfatide with short fatty acid dominates in astrocytes and neurons. *FEBS J,* **273,** 1782-1790.

Ishibashi, T., Dupree, J. L., Ikenaka, K. et al. (2002) A myelin galactolipid, sulfatide, is essential for maintenance of ion channels on myelinated axon but not essential for initial cluster formation. *J Neurosci,* **22,** 6507-6514.

Ishizuka, I., Inomata, M., Ueno, K. and Yamakawa, T. (1978) Sulfated glyceroglycolipids in rat brain. Structure sulfation in vivo, and accumulation in whole brain during development. *J Biol Chem,* **253,** 898-907.

Kadar, H., Pham, H., Touboul, D., Brunelle, A. and Baud, O. (2014) Impact of inhaled nitric oxide on the sulfatide profile of neonatal rat brain studied by TOF-SIMS imaging. *Int J Mol Sci,* **15,** 5233-5245.

Lu, D., Singh, D., Morrow, M. R. and Grant, C. W. (1993) Effect of glycosphingolipid fatty acid chain length on behavior in unsaturated phosphatidylcholine bilayers: a 2H NMR study. *Biochemistry,* **32,** 290-297.

Marbois, B. N., Faull, K. F., Fluharty, A. L., Raval-Fernandes, S. and Rome, L. H. (2000) Analysis of sulfatide from rat cerebellum and multiple sclerosis white matter by negative ion electrospray mass spectrometry. *Biochim Biophys Acta,* **1484,** 59-70.

Miller, R. H. (2002) Regulation of oligodendrocyte development in the vertebrate CNS. *Prog Neurobiol,* **67,** 451-467.

Miller, R. H. and Ono, K. (1998) Morphological analysis of the early stages of oligodendrocyte development in the vertebrate central nervous system. *Microsc Res Tech,* **41,** 441-453.

Norton, W.T. (1977) Isolation and characterization of myelin. In: Morell P, editor. Myelin. New York: Plenum Press. 161–199.

O'Brien, J. S. and Rouser, G. (1964) The fatty acid composition of brain sphingolipids: sphingomyelin, ceramide, cerebroside, and cerebroside sulfate. *J Lipid Res,* **5,** 339-342.

Olivier, C., Cobos, I., Perez Villegas, E. M., Spassky, N., Zalc, B., Martinez, S. and Thomas, J. L. (2001) Monofocal origin of telencephalic oligodendrocytes in the anterior entopeduncular area of the chick embryo. *Development,* **128,** 1757-1769.

Olivier, P., Loron, G., Fontaine, R. H. et al. (2010) Nitric oxide plays a key role in myelination in the developing brain. *J Neuropathol Exp Neurol,* **69,** 828-837.

Ono, K., Bansal, R., Payne, J., Rutishauser, U. and Miller, R. H. (1995) Early development and dispersal of oligodendrocyte precursors in the embryonic chick spinal cord. *Development,* **121,** 1743-1754.

Ono, K., Fujisawa, H., Hirano, S., Norita, M., Tsumori, T. and Yasui, Y. (1997) Early development of the oligodendrocyte in the embryonic chick metencephalon. *J Neurosci Res,* **48,** 212-225.

Ono, K., Kagawa, T., Tsumori, T., Yokota, S. and Yasui, Y. (2001) Morphological changes and cellular dynamics of oligodendrocyte lineage cells in the developing vertebrate central nervous system. *Dev Neurosci,* **23,** 346-355.

Ozgen, H., Schrimpf, W., Hendrix, J., de Jonge, J. C., Lamb, D. C., Hoekstra, D., Kahya, N. and Baron, W. (2014) The lateral membrane organization and dynamics of myelin proteins

PLP and MBP are dictated by distinct galactolipids and the extracellular matrix. *PLoS One,* **9,** e101834.

Pernber, Z., Richter, K., Mansson, J. E. and Nygren, H. (2007) Sulfatide with different fatty acids has unique distributions in cerebellum as imaged by time-of-flight secondary ion mass spectrometry (TOF-SIMS). *Biochim Biophys Acta,* **1771,** 202-209.

Pringle, N. P. and Richardson, W. D. (1993) A singularity of PDGF alpha-receptor expression in the dorsoventral axis of the neural tube may define the origin of the oligodendrocyte lineage. *Development,* **117,** 525-533.

Romero-Perez, G. A., Takei, S. and Yao, I. (2014) Imaging Mass Spectrometric Analysis of Neurotransmitters: A Review. *Mass Spectrom (Tokyo),* **3,** S0049.

Rosenberg, A. and Stern, N. (1966) Changes in sphingosine and fatty acid components of the gangliosides in developing rat and human brain. *J Lipid Res,* **7,** 122-131.

Shroff, S. M., Pomicter, A. D., Chow, W. N., Fox, M. A., Colello, R. J., Henderson, S. C. and Dupree, J. L. (2009) Adult CST-null mice maintain an increased number of oligodendrocytes. *J Neurosci Res,* **87,** 3403-3414.

Sjövall, P., Lausmaa, J. and Johansson, B. (2004) Mass spectrometric imaging of lipids in brain tissue. *Anal Chem,* **76,** 4271-4278.

Sommer, I. and Schachner, M. (1981) Monoclonal antibodies (O1 to O4) to oligodendrocyte cell surfaces: an immunocytological study in the central nervous system. *Dev Biol,* **83,** 311-327.

Sosnik, A., Sodhi, R. N., Brodersen, P. M. and Sefton, M. V. (2006) Surface study of collagen/poloxamine hydrogels by a 'deep freezing' ToF-SIMS approach. *Biomaterials,* **27,** 2340-2348.

Spassky, N., Goujet-Zalc, C., Parmantier, E. et al. (1998) Multiple restricted origin of oligodendrocytes. *J Neurosci,* **18,** 8331-8343.

Stewart, R. J. and Boggs, J. M. (1993) A carbohydrate-carbohydrate interaction between galactosylceramide-containing liposomes and cerebroside sulfate-containing liposomes: dependence on the glycolipid ceramide composition. *Biochemistry,* **32,** 10666-10674.

Svennerholm, L. and Ställberg-Stenhagen, S. (1968) Changes in the fatty acid composition of cerebrosides and sulfatides of human nervous tissue with age. *J Lipid Res,* **9,** 215-225.

van Zyl, R., Gieselmann, V. and Eckhardt, M. (2010) Elevated sulfatide levels in neurons cause lethal audiogenic seizures in mice. *J Neurochem,* **112,** 282-295.

Wada, T., Kagawa, T., Ivanova, A., Zalc, B., Shirasaki, R., Murakami, F., Iemura, S., Ueno, N. and Ikenaka, K. (2000) Dorsal spinal cord inhibits oligodendrocyte development. *Dev Biol*, **227,** 42-55.

Wang, H. Y., Jackson, S. N., Post, J. and Woods, A. S. (2008) A Minimalist Approach to MALDI Imaging of Glycerophospholipids and Sphingolipids in Rat Brain Sections. *Int J Mass Spectrom*, **278,** 143-149.

Yamada, M., Kagawa, T. and Ikenaka, K. (1996) Development and differentiation of oligodendrocytes. *Jpn J Physiol*, **46,** 105-110.

Yuki, D., Sugiura, Y., Zaima, N., Akatsu, H., Hashizume, Y., Yamamoto, T., Fujiwara, M., Sugiyama, K. and Setou, M. (2011) Hydroxylated and non-hydroxylated sulfatide are distinctly distributed in the human cerebral cortex. *Neuroscience*, **193,** 44-53.

Compound	Molecular species	*m/z* values (observed)	*m/z* values (reference)
C16 Sulfatide	*d*18:1-N16:0	778.490	778.51
C16-OH Sulfatide	*d*18:1-OHN16:0	794.485	794.51
C18 Sulfatide	*d*18:1-N18:0	806.546	806.55
C18-OH Sulfatide	*d*18:1-OHN18:0	822.515	822.54
C22 Sulfatide	*d*18:1-N22:0	862.574	862.61
C22-OH Sulfatide	*d*18:1-OHN22:0	878.589	878. 60
C24:1 Sulfatide	*d*18:1-N24:1	888.624	888.62
C24 Sulfatide	*d*18:1-N24:0	890.640	890.64
C24:1-OH Sulfatide	*d*18:1-OHN24:1	904.662	904.62
C24 -OH Sulfatide	*d*18:1-OHN24:0	906.669	906.63
C26:1 Sulfatide	*d*18:1-N26:1	916.711	916.65
C26 Sulfatide	*d*18:1-N26:0	920.706	920.69

Table

Exact mass values of the sulfatide species in the reference standard by iMScope

The standard sulfatides from bovine brains were analyzed with 9AA on a negative ion mode by iMScope. The exact mass values in the reference standard by iMScope were compared with the measured values in the reference (Cheng et al., 2010). *d*: 2-amino-4-octadecene-1,3-diol; N: the prefix for the fatty acyl amide chain; OHN: hydroxyl fatty acyl amide chain.

Figure legends

Fig. 1

Schematic summary of oligodendrocyte lineage *in vitro*.

Specific antibodies to sphingolipids are used for the morphological identification of each oligodendrocyte stage.

Fig. 2

MALDI-MS spectra of a sulfatide reference standard. Mixtures of sulfatide species with various fatty acid chains from bovine brains were analyzed with 9AA in a negative ion mode by iMScope. The averaged mass spectra are shown. There are various sulfatide fatty acid species with nonhydroxy and hydroxyl fatty acids, as well as chain saturated and monounsaturated fatty acids that contain 16 to 26 carbons. The sphingosine base is 2-amino-4-octadecene-1,3-diol for all species in the adult bovine brain and rat brain (Rosenberg and Stern, 1966).

Fig. 3

The major sulfatide species are absent in the Cst-null brain. (A) Comparison of mass spectra of sulfatide species between Cst-null and wild type adult murine brains. (B) Images from the iMScope data indicate that the signaling that results from the sulfatide species disappears in the

Cst -/- brain. The color scale indicates the intensity of the signal from black (low or no signal) to red (strongest signal). (C) Comparison of the sulfatide signal intensity in corpus callosum in 11-week-old wild and CST-null mouse. The statistical comparisons of the values of signal intensity from control vs. CST-null was performed by Student's t-test.

Fig. 4

POA was detected with the DI8 sulfatide-reactive antibody. (A) To determine whether DI8 could substitute for O4, the specificity of D18 was examined. D18-positive cells (green) exist in restricted regions of the ventricular zone of the spinal cord in the stage 32 chick embryo (a, b). Scale bar: 100 μm. The nucleus (blue) is stained with Hoechst 33258. (B) Pro-oligodendroblasts derived from rat brains. The images of the cells stained with DI8 (green) and O4 (magenta) were completely matched (a-c), whereas the images with D18 (green) and O1 (magenta) were partially merged (arrows in d-f). Scale bar: 20 μm. In methanol-treated pro-oligodendroblasts, the DI8 antigen disappeared (h, i) but the GST-π protein (magenta) was present (g, i). Scale bar: 50 μm. (C) E18.5 rat-derived OPCs were purified and cultured for one day under differentiation conditions. Pro-oligodendroblasts were analyzed using a FACS Aria flow cytometer, and the cells were sorted using the Forward Scatter (FSC) and Side Scatter (SSC) (a). The sorted cells

were cultured for 1 day (b). Based on the DI8 (green) and O1 (magenta) antibodies, P1 exhibits immature oligodendrocytes (D18+/O1-), and P3 exhibits mature oligodendrocytes (D18+/O1+) (b). P2 phase contrast (D18-/O1-). Scale bar: 50 μm. After double labeling of population P1 with Cy5-O1 and Alexa 488-DI8, cells were divided into three sub-populations—P4, ($DI8^{low}$ $O1^{low}$; red), P5 ($DI8^{high}$ $O1^{low}$; blue), and P6 ($DI8^{high}$ $O1^{high}$; green) (c). The extract from the P5 population was analyzed for the sulfatide species using a 9AA matrix by iMScope and was demonstrated to contain *m/z* 806.53 and *m/z* 822.51 (d).

Fig. 5

The short-chain sulfatide with 16 and 18 carbon atoms in a defined area of OPC production. (A) Comparison of the mass spectra of the sulfatide species in the stage 32 chick spinal cord by iMScope. The spectra indicate ions that correspond to sulfatide species with 16, 18 and 18-OH carbon atoms (red arrows) and PS and PI (green arrows). (B) Comparison of the immunostaining analysis with the O4 antibody (a, b) to images of sulfatide species with various fatty acid chains from the iMScope-based data analysis (c-j). The analyzed area indicates ionization for each target molecule (d-j). Optical image (c) of d-h and phosphatidylinositol (PI) (38:4) at *m/z* 885.5 (d). e-j indicate sulfatide-related peaks, which are localized to the ventral

ventricular zone as demonstrated by the O4 staining (a). The images for *m/z* 806.5 (i) and *m/z* 834.5 (PS) (j) are obtained in areas that are distinct from those that contain sulfatide in c-h. The *m/z* 806.5 imaging signal is significantly localized to a restricted area (i), whereas the *m/z* 834.52 is spread along the dorsoventral axis (j).

(C) iMSCope-based images of the sulfatide species (c-f) correspond to the immunoreactivity of the Olig2 OPC marker (green) in the stage 37 chick spinal cord (b). (a) Hoechst staining (blue). Scale bar: 100 μm. Color scale indicates the intensity of the signal from black (low or no signal) to red (strongest signal).

Fig. 6

Evaluation of the *m/z* 806.5 ion mass spectra. (A) Mass spectra of the *m/z 806.5* ion from the embryonic stage 32 chick spinal cord (b) and adult murine brain (a) by iMScope. (B) Tandem mass spectrometry analysis of the *m/z* 806.5 ion from the embryonic stage 32 chick spinal cord (b) and adult murine brain (a) by iMScope. The major fragments that appear in both tissues are marked with a red arrow. The parent ion at *m/z* 807.5 represents the isotope variants of the *m/z* 806.5 ions.

Fig. 7

Sulfatide species in the murine spinal cord and brain at multiple embryonic stages by iMScope. (A) Cervical spinal cord (a-f), medulla (g, h) and pons (i, j) at stage E15.5. The C16, C18, C18-OH and C22-OH sulfatide species were identified in restricted areas of the spinal cord (a-f), and the C18-OH sulfatide was detected in the medulla (g, h) and pons (i, j). (B) Medulla (a-d), pons (e-g) and midbrain (i-l) at stage E18.5. The sulfatide species signal gradually expanded from the restricted region to the lateral part of the medulla (a-c) and pons (e-g). However, it was not present in the midbrain (i-l). (C) Spinal cord on E19.5. In addition to the C18-OH sulfatide, the C22-OH sulfatide appeared in the ventral zone of the spinal cord. The C24 monounsaturated sulfatide at *m/z* 888.6 was absent from all regions at all stages (A-f, B-d, h, l, C-d). The color scale indicates the intensity of the signal from black (low or no signal) to red (strongest signal).

Fig. 8

TOF−SIMS images of ions from a freeze-dried murine brain section. (A) The 5 mm x 3 mm section (a) was obtained from the measurement of the negative mode. A magnified image of a 500-μm field of view (FOV) in the black square in area a (Scale bar: 100 μm) was obtained. A 200-μm FOV in area b was obtained by the white square in area a (b, Scale bar: 100 μm). The spatial intensity distributions of the PO_3 ion (green) and cholesterol at *m/z* 385 (red) are shown

(a, b). The serial section was immunostained with MBC (green) and Olig 2 (magenta), and the nuclei were stained with Hoechst (blue) (c, d, Scale bar: 200 μm). High magnification (d). Sulfatide spectra from the corpus callosum area in area b (e) and isotope peaks (f). (B) Images of the ion intensity in area A, b for CNO (a), cholesterol at *m/z* 385 (b), and four sulfatide species at *m/z* 807, *m/z* 823, *m/z* 863 and *m/z* 889 with their isotope variants (c). The merged image indicates CNO (blue), cholesterol (red), and the four sulfatide species (green) (d). The analyzed areas are shown for each sulfatide species, including the *m/z* 807 (e), *m/z* 823 (f), *m/z* 863 (g) and *m/z* 889 (h) isotopes. The *m/z* 807 (red), *m/z* 889 (green) and CNO (blue) ion signals are overlaid (i). The *m/z* 807 (red), *m/z* 823 (green) and *m/z* 863 (blue) ion signals are overlaid (j). Scale bar: 100 μm. (C) High spatial resolution with a 100-μm field of view and 150-nm beam size. Images of CNO (a) and cholesterol at *m/z* 385 (b), along with a magnified image in the white square from area a were obtained (c, d). The merged image indicates CNO (blue), cholesterol (green), and four sulfatide species (red) (d). The *m/z* 807 (red), *m/z* 889 (green) and *m/z* 823 (blue) ion signals, which included each isotope, are overlaid (e). (c, d, e, scale bar: 10 μm)

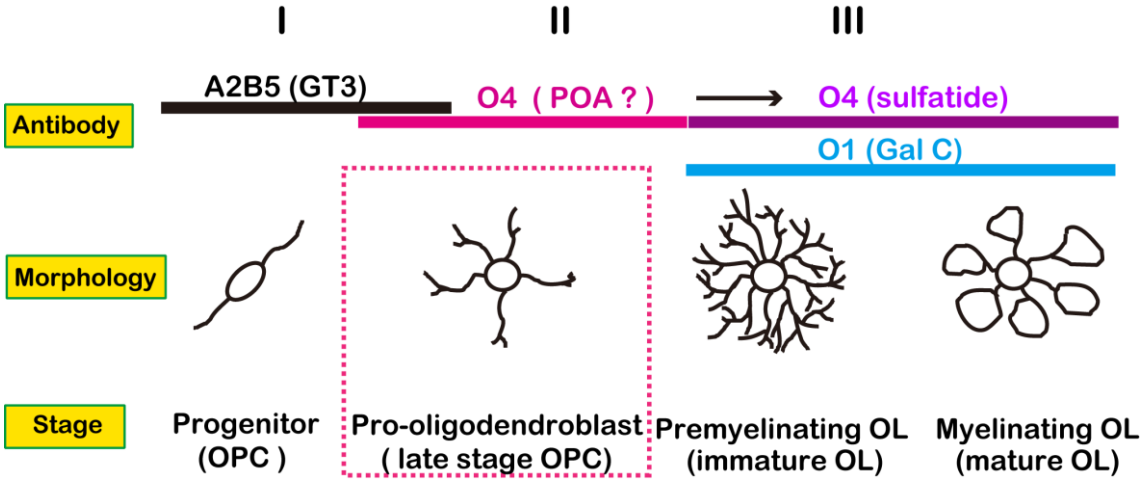

Fig. 1

Schematic summary of oligodendrocyte lineage *in vitro*.

Specific antibodies to sphingolipids are used for the morphological identification of each oligodendrocyte stage.

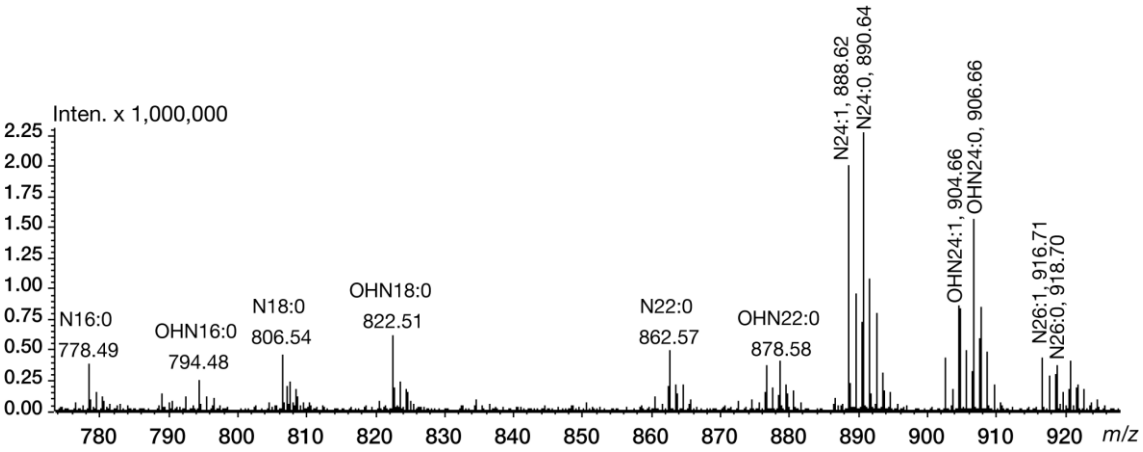

Fig. 2

MALDI-MS spectra of a sulfatide reference standard. Mixtures of sulfatide species with various fatty acid chains from bovine brains were analyzed with 9AA in a negative ion mode by iMScope. The averaged mass spectra are shown. There are various sulfatide fatty acid species with nonhydroxy and hydroxyl fatty acids, as well as chain saturated and monounsaturated fatty acids that contain 16 to 26 carbons. The sphingosine base is 2-amino-4-octadecene-1,3-diol for all species in the adult bovine brain and rat brain (Rosenberg and Stern, 1966).

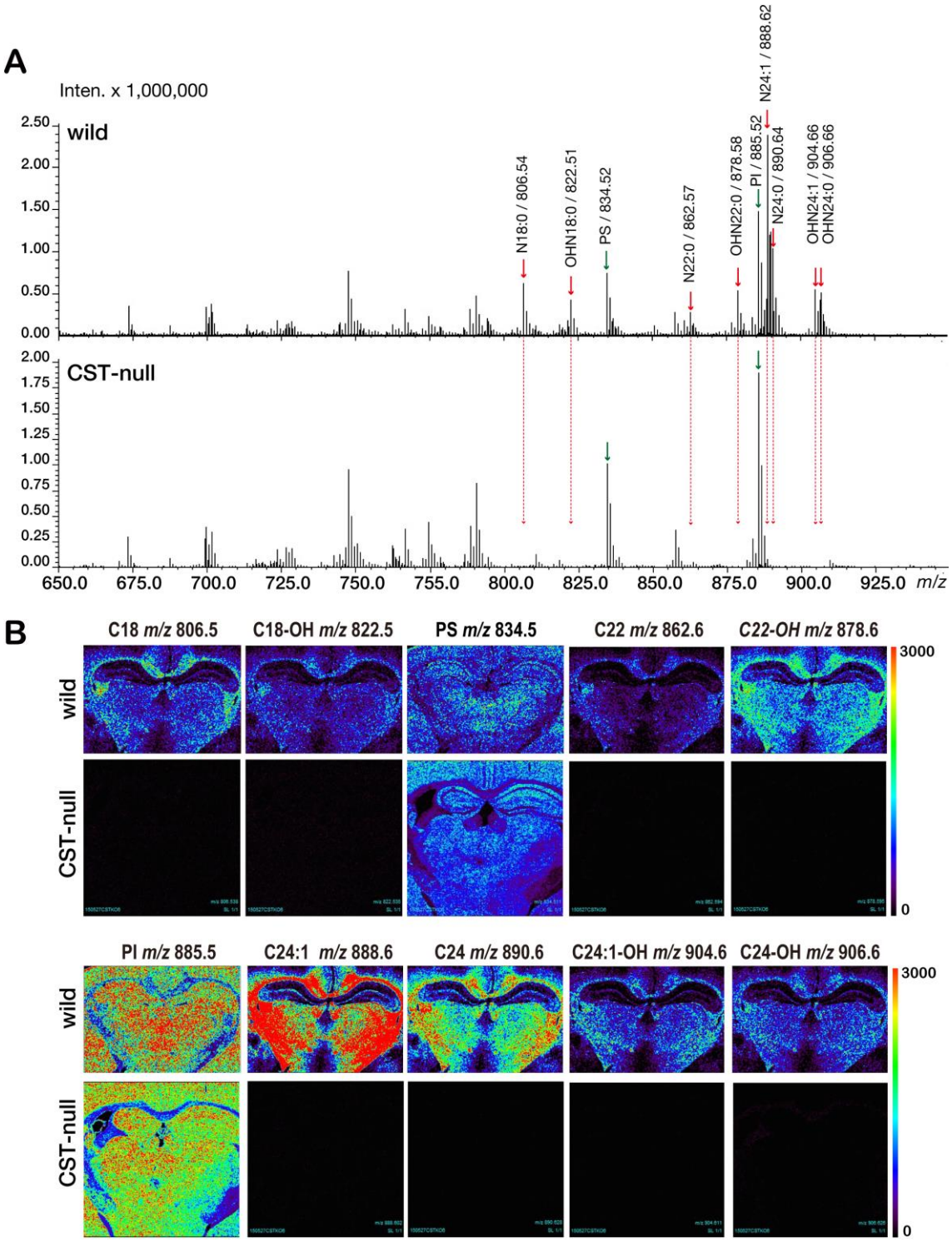
A
Inten. x 1,000,000
wild
CST-null
N18:0 / 806.54
OHN18:0 / 822.51
PS / 834.52
N22:0 / 862.57
OHN22:0 / 878.58
PI / 885.52
N24:1 / 888.62
N24:0 / 890.64
OHN24:1 / 904.66
OHN24:0 / 906.66
m/z
B
C18 m/z 806.5
C18-OH m/z 822.5
PS m/z 834.5
C22 m/z 862.6
C22-OH m/z 878.6
PI m/z 885.5
C24:1 m/z 888.6
C24 m/z 890.6
C24:1-OH m/z 904.6
C24-OH m/z 906.6
3000
0

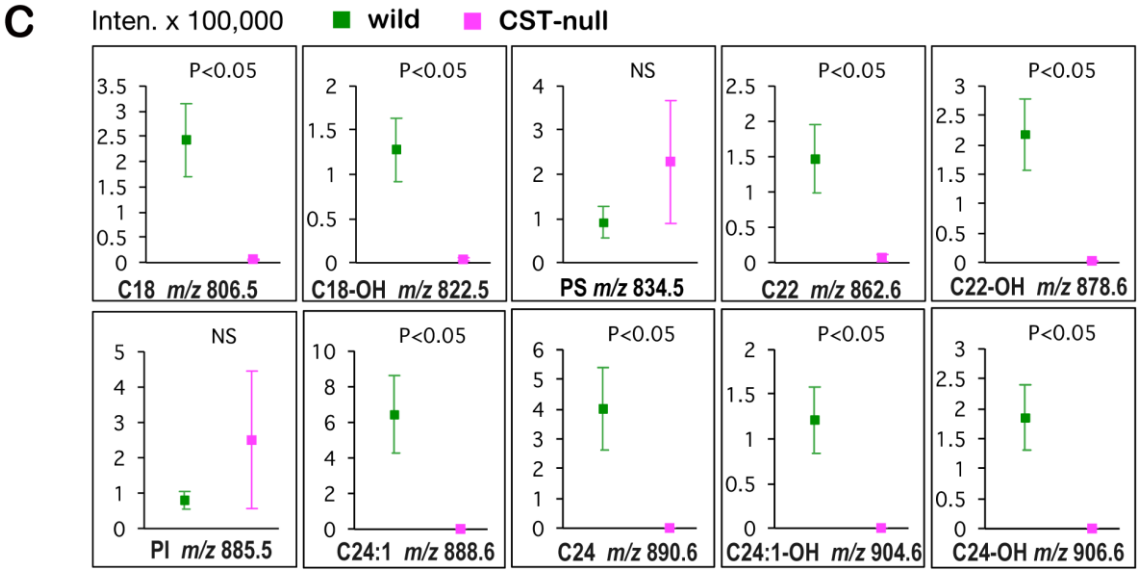

Fig. 3

The major sulfatide species are absent in the Cst-null brain. (A) Comparison of mass spectra of sulfatide species between Cst-null and wild type adult murine brains. (B) Images from the iMScope data indicate that the signaling that results from the sulfatide species disappears in the Cst -/- brain. The color scale indicates the intensity of the signal from black (low or no signal) to red (strongest signal). (C) Comparison of the sulfatide signal intensity in corpus callosum in 11-week-old wild and CST-null mouse. The statistical comparisons of the values of signal intensity from control vs. CST-null was performed by Student's t-test.

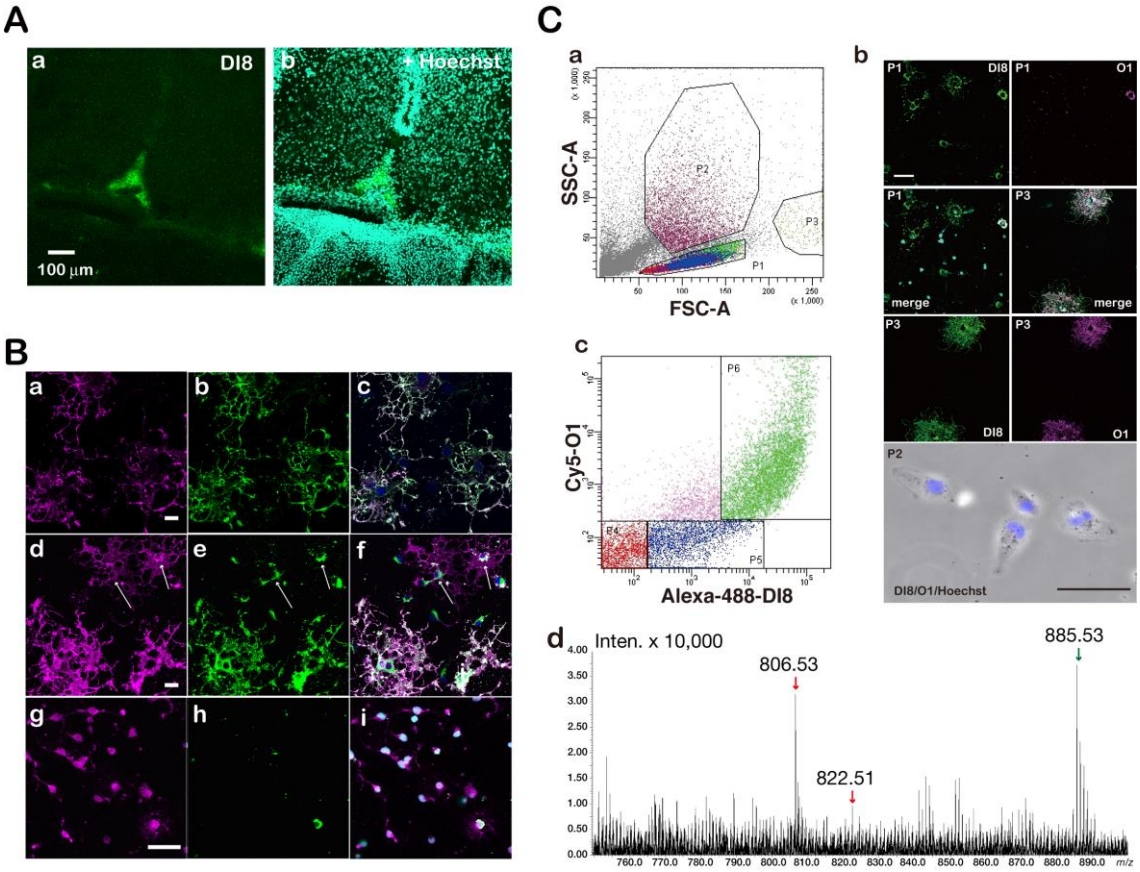

Fig. 4

POA was detected with the DI8 sulfatide-reactive antibody. (A) To determine whether DI8 could substitute for O4, the specificity of D18 was examined. D18-positive cells (green) exist in restricted regions of the ventricular zone of the spinal cord in the stage 32 chick embryo (a, b). Scale bar: 100 μm. The nucleus (blue) is stained with Hoechst 33258. (B) Pro-oligodendroblasts derived from rat brains. The images of the cells stained with DI8 (green) and O4 (magenta) were completely matched (a-c), whereas the images with D18 (green) and O1 (magenta) were partially merged (arrows in d-f). Scale bar: 20 μm. In methanol-treated pro-oligodendroblasts, the DI8 antigen disappeared (h, i) but the GST-π protein (magenta) was present (g, i). Scale bar: 50 μm. (C) E18.5 rat-derived OPCs were purified and cultured for one day under differentiation conditions. Pro-oligodendroblasts were analyzed using a FACS Aria flow cytometer, and the cells were sorted using the Forward Scatter (FSC) and Side Scatter (SSC) (a). The sorted cells were cultured for 1 day (b). Based on the DI8 (green) and O1 (magenta) antibodies, P1 exhibits immature oligodendrocytes (D18+/O1-), and P3 exhibits mature oligodendrocytes (D18+/O1+) (b). P2 phase contrast (D18-/O1-). Scale bar: 50 μm. After double labeling of population P1 with Cy5-O1 and Alexa 488-DI8, cells were divided into three sub-populations—P4, (DI8^{low}

$O1^{low}$; red), P5 ($DI8^{high}$ $O1^{low}$; blue), and P6 ($DI8^{high}$ $O1^{high}$; green) (c). The extract from the P5 population was analyzed for the sulfatide species using a 9AA matrix by iMScope and was demonstrated to contain *m/z* 806.53 and *m/z* 822.51 (d).

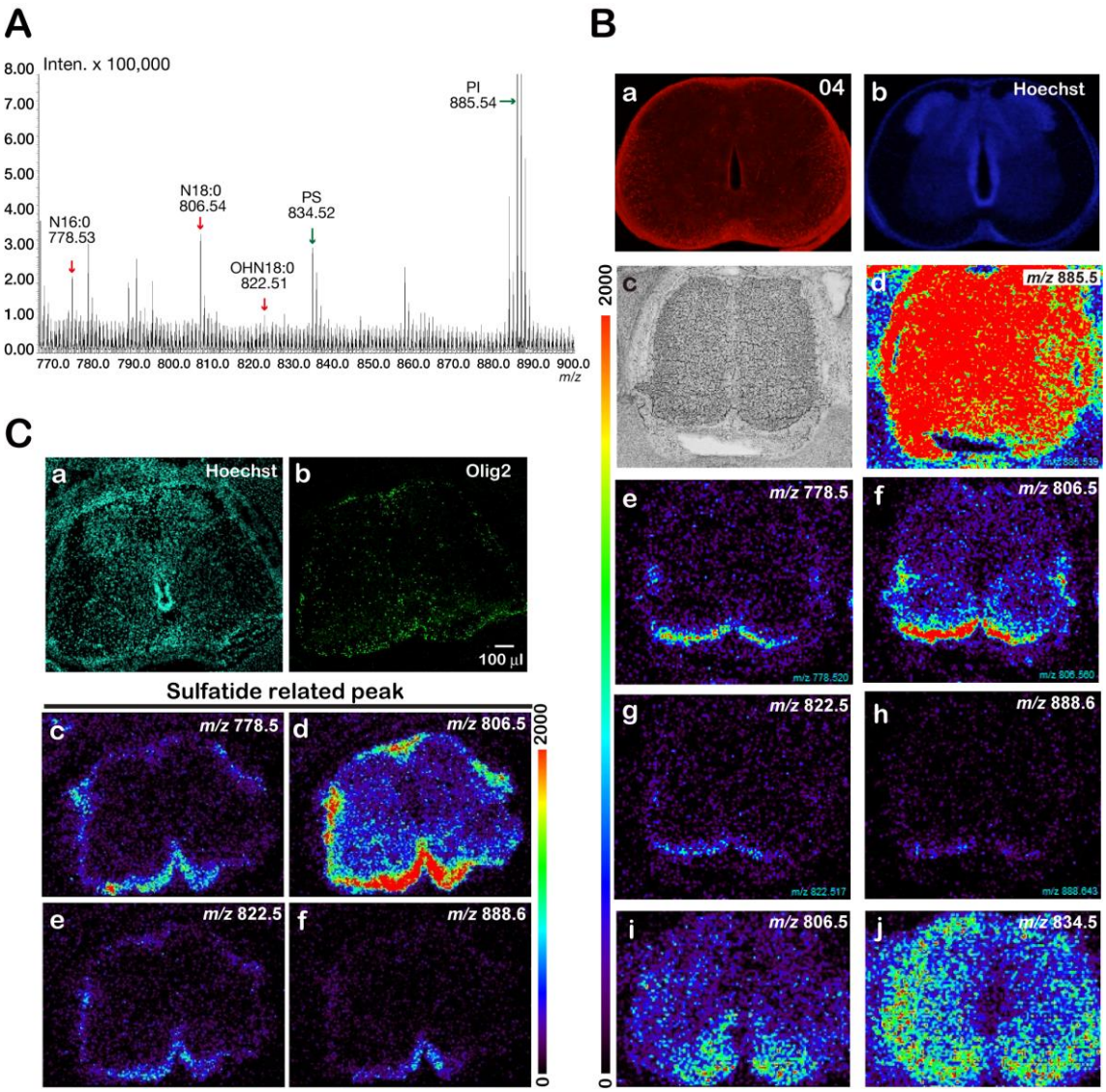

Fig. 5

The short-chain sulfatide with 16 and 18 carbon atoms in a defined area of OPC production. (A) Comparison of the mass spectra of the sulfatide species in the stage 32 chick spinal cord by iMScope. The spectra indicate ions that correspond to sulfatide species with 16, 18 and 18-OH carbon atoms (red arrows) and PS and PI (green arrows). (B) Comparison of the immunostaining analysis with the O4 antibody (a, b) to images of sulfatide species with various fatty acid chains from the iMScope-based data analysis (c-j). The analyzed area indicates ionization for each target molecule (d-j). Optical image (c) of d-h and phosphatidylinositol (PI) (38:4) at *m/z* 885.5 (d). e-j indicate sulfatide-related peaks, which are localized to the ventral ventricular zone as demonstrated by the O4 staining (a). The images for *m/z* 806.5 (i) and *m/z* 834.5 (PS) (j) are obtained in areas that are distinct from those that contain sulfatide in c-h. The

m/z 806.5 imaging signal is significantly localized to a restricted area (i), whereas the *m/z* 834.52 is spread along the dorsoventral axis (j).

(C) iMSCope-based images of the sulfatide species (c-f) correspond to the immunoreactivity of the Olig2 OPC marker (green) in the stage 37 chick spinal cord (b). (a) Hoechst staining (blue). Scale bar: 100 μm. Color scale indicates the intensity of the signal from black (low or no signal) to red (strongest signal).

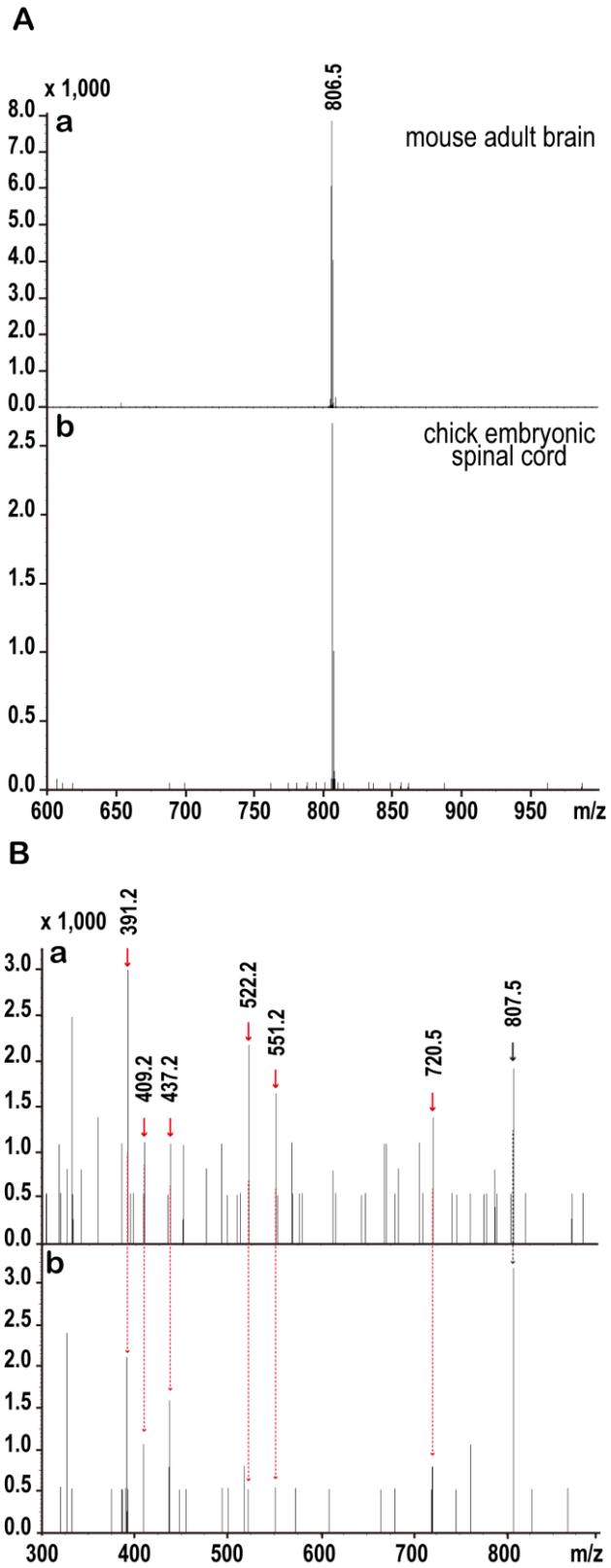

Fig. 6

Evaluation of the *m/z* 806.5 ion mass spectra. (A) Mass spectra of the *m/z 806.5* ion from the

embryonic stage 32 chick spinal cord (b) and adult murine brain (a) by iMScope. (B) Tandem mass spectrometry analysis of the *m/z* 806.5 ion from the embryonic stage 32 chick spinal cord (b) and adult murine brain (a) by iMScope. The major fragments that appear in both tissues are marked with a red arrow. The parent ion at *m/z* 807.5 represents the isotope variants of the *m/z* 806.5 ions.

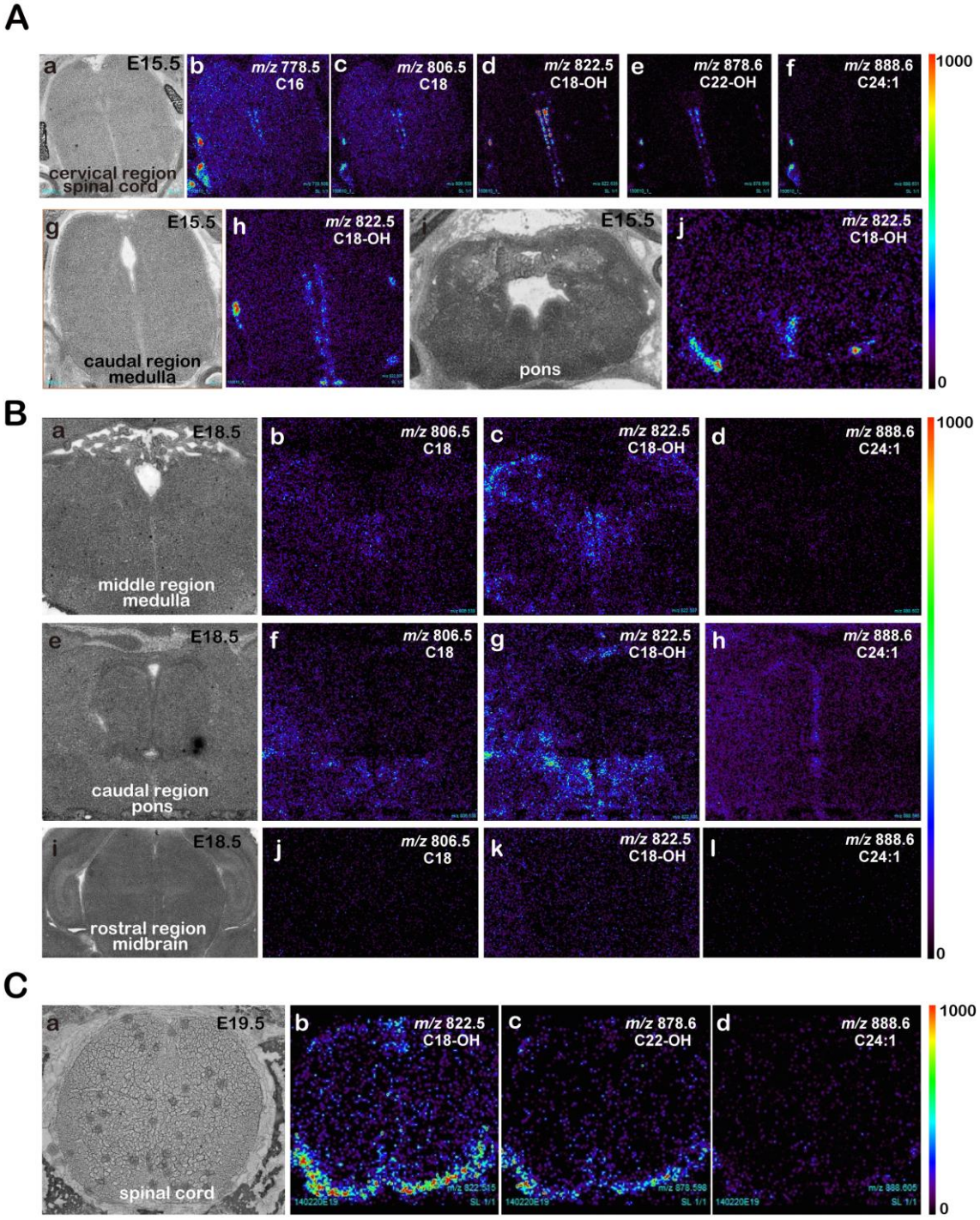

Fig. 7

Sulfatide species in the murine spinal cord and brain at multiple embryonic stages by iMScope. (A) Cervical spinal cord (a-f), medulla (g, h) and pons (i, j) at stage E15.5. The C16, C18, C18-OH and C22-OH sulfatide species were identified in restricted areas of the spinal cord (a-f), and the C18-OH sulfatide was detected in the medulla (g, h) and pons (i, j). (B) Medulla (a-d), pons (e-g) and midbrain (i-l) at stage E18.5. The sulfatide species signal gradually expanded

from the restricted region to the lateral part of the medulla (a-c) and pons (e-g). However, it was not present in the midbrain (i-l). (C) Spinal cord on E19.5. In addition to the C18-OH sulfatide, the C22-OH sulfatide appeared in the ventral zone of the spinal cord. The C24 monounsaturated sulfatide at *m/z* 888.6 was absent from all regions at all stages (A-f, B-d, h, l, C-d). The color scale indicates the intensity of the signal from black (low or no signal) to red (strongest signal).

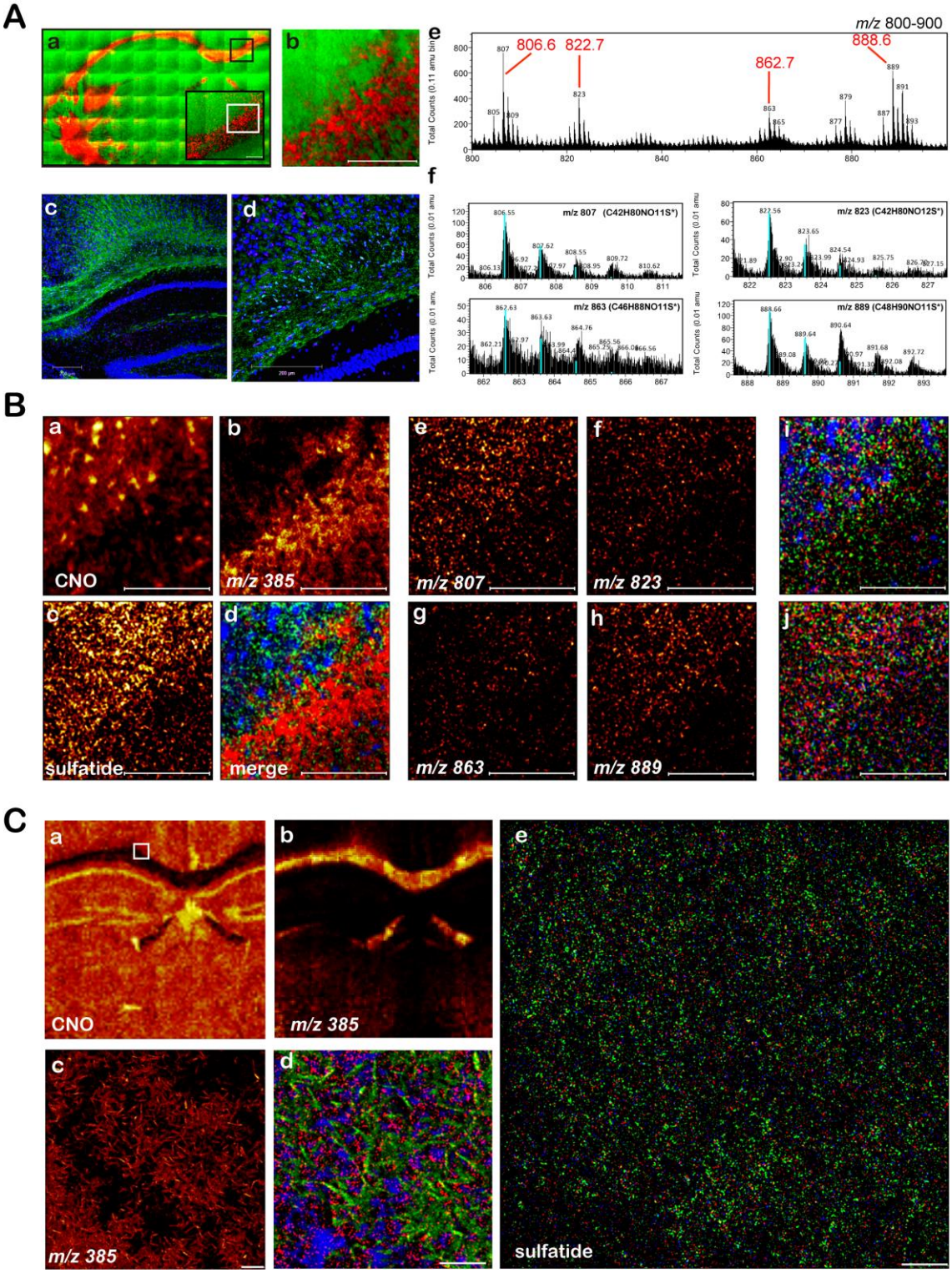

Fig. 8

TOF−SIMS images of ions from a freeze-dried murine brain section. (A) The 5 mm x 3 mm section (a) was obtained from the measurement of the negative mode. A magnified image of a 500-μm field of view (FOV) in the black square in area a (Scale bar: 100 μm) was obtained. A

200-μm FOV in area b was obtained by the white square in area a (b, Scale bar: 100 μm). The spatial intensity distributions of the PO_3 ion (green) and cholesterol at *m/z* 385 (red) are shown (a, b). The serial section was immunostained with MBC (green) and Olig 2 (magenta), and the nuclei were stained with Hoechst (blue) (c, d, Scale bar: 200 μm). High magnification (d). Sulfatide spectra from the corpus callosum area in area b (e) and isotope peaks (f). (B) Images of the ion intensity in area A, b for CNO (a), cholesterol at *m/z* 385 (b), and four sulfatide species at *m/z* 807, *m/z* 823, *m/z* 863 and *m/z* 889 with their isotope variants (c). The merged image indicates CNO (blue), cholesterol (red), and the four sulfatide species (green) (d). The analyzed areas are shown for each sulfatide species, including the *m/z* 807 (e), *m/z* 823 (f), *m/z* 863 (g) and *m/z* 889 (h) isotopes. The *m/z* 807 (red), *m/z* 889 (green) and CNO (blue) ion signals are overlaid (i). The *m/z* 807 (red), *m/z* 823 (green) and *m/z* 863 (blue) ion signals are overlaid (j). Scale bar: 100 μm. (C) High spatial resolution with a 100-μm field of view and 150-nm beam size. Images of CNO (a) and cholesterol at *m/z* 385 (b), along with a magnified image in the white square from area a were obtained (c, d). The merged image indicates CNO (blue), cholesterol (green), and four sulfatide species (red) (d). The *m/z* 807 (red), *m/z* 889 (green) and *m/z* 823 (blue) ion signals, which included each isotope, are overlaid (e). (c, d, e, scale bar: 10 μm)